Mechanisms in non-heme iron oxidation catalysis

Chen, Juan

CHAPTER 6

H_2O_2 Oxidation by Fe^{III}-OOH Intermediates and its Impact on Catalytic Efficiency

The oxidation of the C-H and C=C bonds of hydrocarbons with H_2O_2 catalyzed by non-heme iron complexes with pentadentate ligands is widely accepted as involving a reactive Fe^{IV}=O species such as $[(N4Py)Fe^{IV}=O]^{2+}$ (where N4Py is 1,1-di(pyridin-2-yl)-*N,N*-bis(pyridin-2-ylmethyl)methanamine) formed by homolytic cleavage of the O-O bond of an Fe^{III}-OOH intermediate. We show here that at low H_2O_2 concentrations the Fe^{IV}=O species formed is detectable in methanol. Furthermore we show that the decomposition of H_2O_2 to water and O_2 is an important competing pathway that limits efficiency in terminal oxidant, and indeed dominates reactivity except where only sub/near-stoichiometric amounts of H_2O_2 are present. Although independently prepared $[(N4Py)Fe^{IV}=O]^{2+}$ oxidizes stoichiometric H_2O_2 rapidly, the rate of formation of Fe^{IV}=O from the Fe^{III}-OOH intermediate is too low to account for the rate of H_2O_2 decomposition observed under catalytic conditions. Indeed, contrary to expectations, with excess H_2O_2, disproportionation to O_2 and H_2O is catalyzed by the Fe(III)-OOH intermediate, and not the Fe^{IV}=O species. These data reveal that the activity of these catalysts with respect to hydrocarbon/alkene oxidation is maximized by maintaining sub/near-stoichiometric steady state concentrations of H_2O_2, which ensure that the rate of the H_2O_2 oxidation by the Fe^{III}-OOH intermediate is less than the rate of the O-O bond homolysis and the subsequent reaction of the Fe^{IV}=O species with substrate.

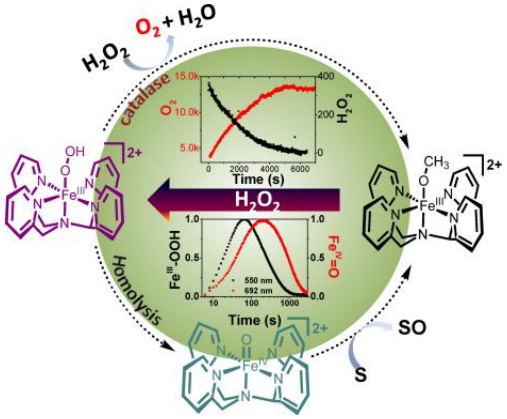

Manuscript has been submitted:

Juan Chen, Apparao Draksharapu, Davide Angelone, Duenpen Unjaroen, Sandeep K. Padamati, Ronald Hage, Carole Duboc, Marcel Swart, Wesley R. Browne

6.1 Introduction

Biomimetic analogs play a central role in understanding bioinorganic systems and enzymes, particularly in the identification of reactive intermediates and their role in catalytic processes.[1–4] In this context, high valent iron oxo species (i.e. Fe^{IV}=O) have been studied intensively over the last decade,[5–9] especially since their first isolation and crystallographic characterization by Que and co-workers in 2003[10]. Indeed, the synthetic non-heme Fe^{IV}=O complexes reported to date, show a broad range of reactivity including C-H oxidation[11–15] with potencies comparable to non-heme and heme enzymes, such as Tau-D, and cytochrome P450.[16]

Isolated Fe^{IV}=O species are invaluable in determining their intrinsic reactivity. High valent Fe^{IV}=O species are frequently invoked as the active species engaged in the oxidation of organic substrates by both heme and non-heme enzymes.[3,5,7,17,18] The continuous regeneration of Fe^{IV}=O under catalytic conditions, with H_2O_2 as terminal oxidant, is desirable also in achieving turnover in the oxidative transformations that they engage in.

The formation of Fe^{IV}=O species upon homolytic O-O bond cleavage in their corresponding Fe^{III}-OOH complexes has been postulated to be a key step for the oxidation of organic substrates by non-heme iron catalysts with H_2O_2.[3,4,19] For example, in the oxidative cleavage of DNA by bleomycin-Fe^{III}-OOH.[20,21] However, to the best of our knowledge, this process (Fe^{III}-OOH $\rightarrow$ Fe^{IV}=O) has not been observed directly for low-spin Fe^{III}-OOH complexes, and was described only recently for high spin Fe^{III}-OOH species.[22–26] Furthermore, the relatively low efficiency of non-heme iron complexes in alkane oxidations with an excess of H_2O_2, together with the known reactivity of Fe^{IV}=O species with H_2O_2[27] castes doubt over the validity of this paradigm under catalytic conditions.[3]

The absence of evidence of the formation of Fe^{IV}=O species and loss of H_2O_2 through unproductive pathways (i.e. disproportionation) can be rationalized by assuming that the generated Fe^{IV}=O species either reacts with H_2O_2 or engages in, e.g., C-H oxidation. Such a mechanism requires that the rate of reaction of Fe^{IV}=O species with H_2O_2 is similar to that with an organic substrate. Iron(III) complexes, such as the Fe^{III}(TAML) (TAML = tetra-amidato-macrocyclic-ligand) system reported by Collins and co-workers, disproportionate H_2O_2 through a Fe^{IV}=O intermediate[2] implying that oxidation of H_2O_2 is rapid compared with C-H oxidation. Indeed data obtained with isolated $[(N4Py)Fe^{IV}=O]^{2+}$ complex (N4Py is 1,1-di(pyridin-2-yl)-*N,N*-bis(pyridin-2-ylmethyl)methanamine) indicates that H_2O_2 oxidation proceeds much more rapidly than C-H oxidation.[27]

In the case of complexes based on pentadentate ligands, e.g., N4Py, the apparent stability of the Fe^{III}-OOH intermediate and absence of direct spectroscopic evidence for the formation of Fe^{IV}=O from this intermediate, make it challenging to identify the actual mechanisms involved in substrate oxidation and H_2O_2 disproportionation.

Here, using a combination of time resolved UV-vis absorption, (resonance) Raman and EPR spectroscopy and computational chemistry, we demonstrate that, contrary to expectations, the rate of O-O bond homolysis in $[(N4Py)Fe^{III}\text{-}OOH]^{2+}$ to form $[(N4Py)Fe^{IV}=O]^{2+}$ and a hydroxyl radical is much lower than the rate of H_2O_2 disproportionation observed under reaction conditions. We show that it is the Fe(III)-OOH species that is responsible for H_2O_2 decomposition and as a result the efficiency of substrate oxidation is negatively affected by an increase in the steady state H_2O_2 concentration, since formation of Fe^{IV}=O species is uncompetitive.

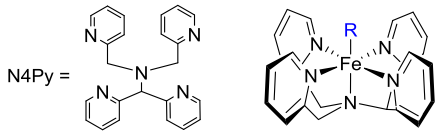

$[(N4Py)Fe^{II}(CH_3CN)]^{2+}$ (**1**) $[(N4Py)Fe^{II}(OCH_3)]^{+}$ (**2**)

$[(N4Py)Fe^{III}(OOH)]^{2+}$ (**3**) $[(N4Py)Fe^{IV}(O)]^{2+}$ (**4**)

$[(N4Py)Fe^{III}(OCH_3)]^{2+}$ (**5a**) $[(N4Py)Fe^{III}(OH)]^{2+}$ (**5b**)

Figure 100. Structures of the complexes and intermediates discussed in the present study.

6.2 Results and Discussion

Typically, acetonitrile is the solvent of choice for the reaction of non-heme iron complexes with oxidants such as H_2O_2. However, in acetonitrile, the formation of $[(N4Py)Fe^{III}\text{-}OOH]^{2+}$ (**3**) is observed only with a stoichiometric excess (> 50 equiv) of H_2O_2 and the subsequent formation of $[(N4Py)Fe^{IV}{=}O]^{2+}$ (**4**) has not been observed,[21] despite that **4**, prepared independently, is itself stable in acetonitrile even at room temperature. In the present study methanol is chosen to circumvent the formation of kinetically inert CH_3CN complexes such as $[(N4Py)Fe^{II}\text{-}NCCH_3]^{+}$ (**1**). The CH_3CN ligand of **1** exchanges immediately with methanol, to form $[(N4Py)Fe^{II}\text{-}OCH_3]^{+}$ (**2**), manifested in a decrease and red shift in the near-UV and visible absorption bands (**Figure 101**).[28] The exchange of the methoxido ligand for water and H_2O_2 is relatively rapid in both the ferrous and ferric states (vide infra), which is central to enabling observation of other species involved in the reactions discussed and is in stark contrast to the slow ligand exchange seen for **1** in acetonitrile.

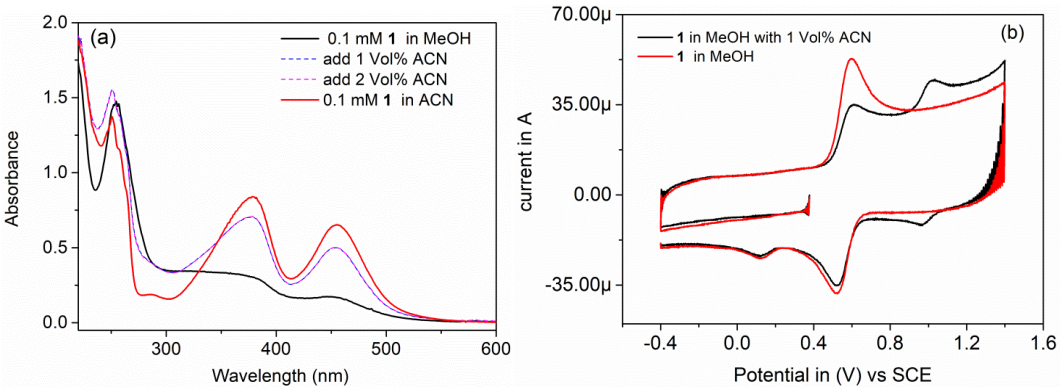

Figure 101. (left) UV-vis absorption spectrum of **1** (0.1 mM) in methanol and in acetonitrile and after addition of acetonitrile to a solution of **1** in methanol (dashed lines); (right) Cyclic voltammetry of **1** (1 mM) in methanol (0.1 M TBA(OTf)) (red line) and after addition of 1 vol % acetonitrile (black line).

6.2.1 Reaction of 1 with stoichiometric H_2O_2 and homolysis of O-O bond of $[(N4Py)Fe^{III}\text{-}OOH]^{2+}$

Addition of 0.6 equiv of H_2O_2 to **2** results in immediate (< 2 s) conversion to $[(N4Py)Fe^{III}\text{-}OCH_3)]^{2+}$ (**5a**) with its characteristic X-Band EPR spectrum at g = 2.29, 2.12, and 1.96.[29] With 1.2 equiv of H_2O_2, $[(N4Py)Fe^{III}(OOH)]^{2+}$ (**3**) is obtained in minor amounts both by UV/Vis absorption and EPR spectroscopy (g = 2.16, 2.11 and 1.98,[21] **Figure 102**). Addition of 2 equiv H_2O_2 to **2** results in the formation of $[(N4Py)Fe^{III}(OOH)]^{2+}$ (**3**) (**Figure 103**) by ligand exchange over 50 s at room temperature reaching a maximum of 14% (based on the absorbance at 550 nm, **Figure 103**-I)

before decreasing again over 1000 s. The decrease in absorbance at 550 nm (of **3**) proceeds concomitant with an increase in absorbance at 692 nm due to Fe^{IV}=O (**4, Figure 103**-II/III). **4** reacts rapidly (200 s) with even stoichiometric H_2O_2 (vide infra) and, therefore, its appearance indicates that the concentration of H_2O_2 in solution is already negligible by 80 s (vide infra). The absorbance at 692 nm remains almost constant over 200 s during the decay of **3**, before decreasing also concomitant with formation of more $[(N4Py)Fe^{III}\text{-}OCH_3]^{2+}$ (**5a**). These data are consistent with equilibration between **5a** and **3** followed by O-O bond homolysis to form **4**, which in the presence of H_2O_2 is reduced to **5a** rapidly. Once sufficient H_2O_2 is consumed the concentration of **4** is determined by the rate of its formation from **3** and the rate of its reaction with methanol (vide infra).

The rate of formation of **4** through homolysis of the O-O bond of $[(N4Py)Fe^{III}\text{-}OOH]^{2+}$ (**3**) under these conditions is low (< 2.2 × 10^{-4} s^{-1}, *vide infra*), which is consistent with the reaction's endergonicity; calculated at 19.1 kcal mol^{-1}. The value is also consistent with the reported value calculated for the related homolytic cleavage in activated Fe-bleomycin.[18,30]

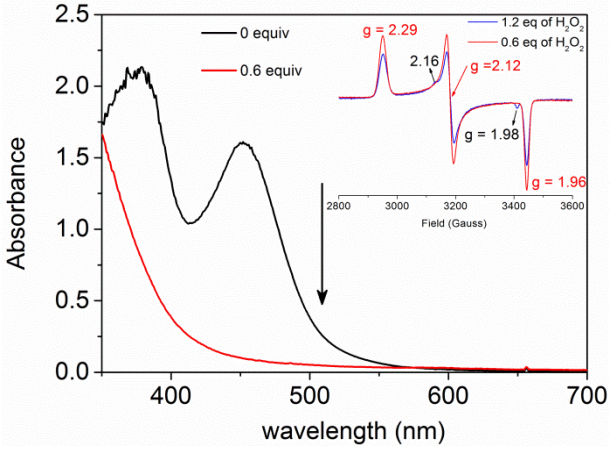

Figure 102. UV-vis absorption spectrum of **1** (0.1 mM) in methanol (black) after addition of 0.6 equiv H_2O_2 (red); Inset shows the X-band EPR spectra for the flash frozen of the corresponding reaction solution at 77 K.

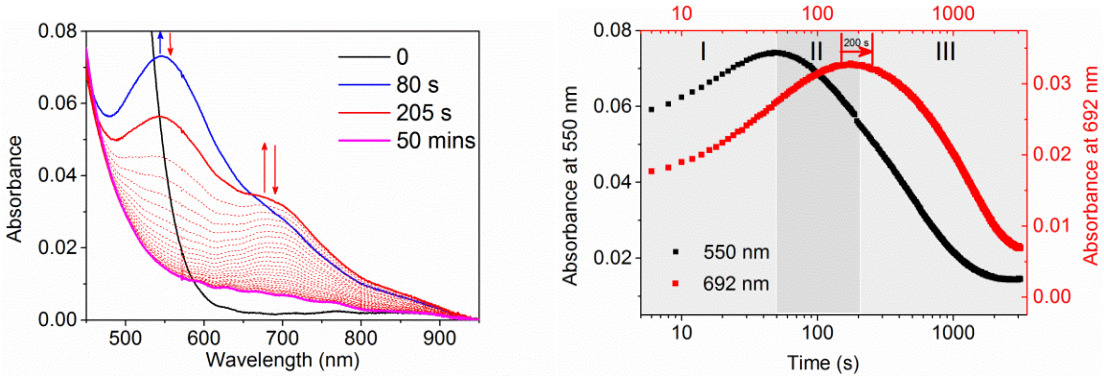

Figure 103. (left) UV-vis absorption spectrum of 2a (0.25 mM) in methanol before (black) and after addition of 2 equiv H_2O_2 at 21 °C. (Right) Corresponding change in absorbance over time at 550 and 692 nm. Pathlength used was 2 cm.

(1) $[(N4Py)Fe^{III}(OOH)]^{2+} \longrightarrow [(N4Py)Fe^{IV}(O)]^{2+} + {}^{\bullet}OH$

ΔG = 19.1 kcal mol^{-1}

6.2.2 Disproportionation of H_2O_2 by 1 in methanol

Addition of excess H_2O_2 (> 40 equiv) to **1** in methanol results in immediate oxidation to **5a** (i.e., a complete loss in absorbance at 450 nm within the mixing time, 2 s; **Figure 104**). The oxidation is followed by full conversion of **5a** to $[(N4Py)Fe^{III}\text{-}OOH)]^{2+}$ (**3**) over 5-10 s. The second order rate constant for the formation of **3** from **5a**, determined under pseudo-first order conditions (2.5 to 50 mM H_2O_2, **Figure 105**), is 10.5 (± 0.1) M^{-1} s^{-1} at 21 °C, consistent with the exothermicity (-10.2 kcal·mol^{-1}) and low barrier for the exchange of the 6th ligand.

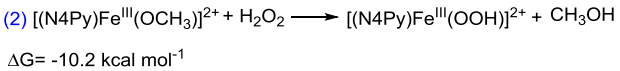

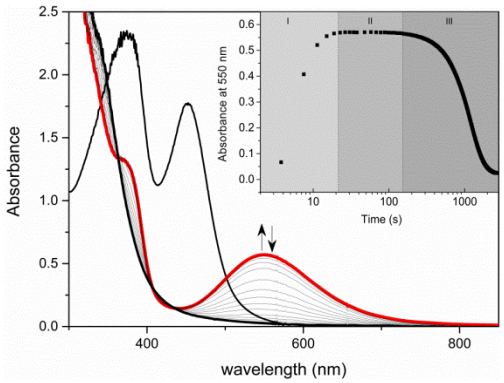

Figure 104. UV-vis absorption spectrum of **1** (0.5 mM) upon addition of 50 equiv H_2O_2. Inset is the corresponding absorbance changing with time.

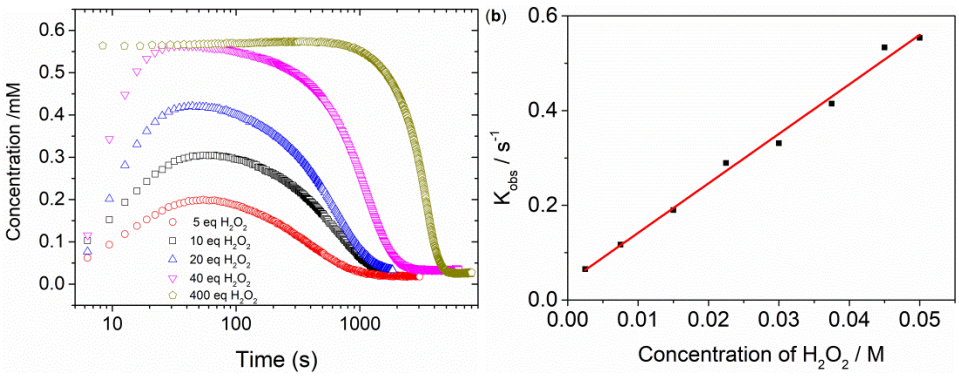

Figure 105. Concentration of $[(N4Py)Fe^{III}\text{-}OOH]^{2+}$ (**3**, from absorbance at 550 nm) against log(time) for various amounts of H_2O_2 added (5 (red), 10 (black), 20 (blue), 40 (pink), and 400 (khaki) equiv) to **1** (0.56 mM) at 21 °C (left). The pseudo-first order rate constant k_{obs} for the formation of $[(N4Py)Fe^{III}\text{-}OOH)]^{2+}$ *vs* concentration of H_2O_2 (right).

EPR spectra of samples flash frozen to 77 K (**Figure 106**) immediately after addition of an excess of H_2O_2 show two well-resolved S = ½ signals, characteristic of **3** (major species) and **5a** (minor species). Samples, flash frozen after 18 min, show that the signals of **3** are diminished with the concomitant increase in the signals of **5a** and at ca. 50 min, the signals of **3** are absent, leaving only those of **5a**.

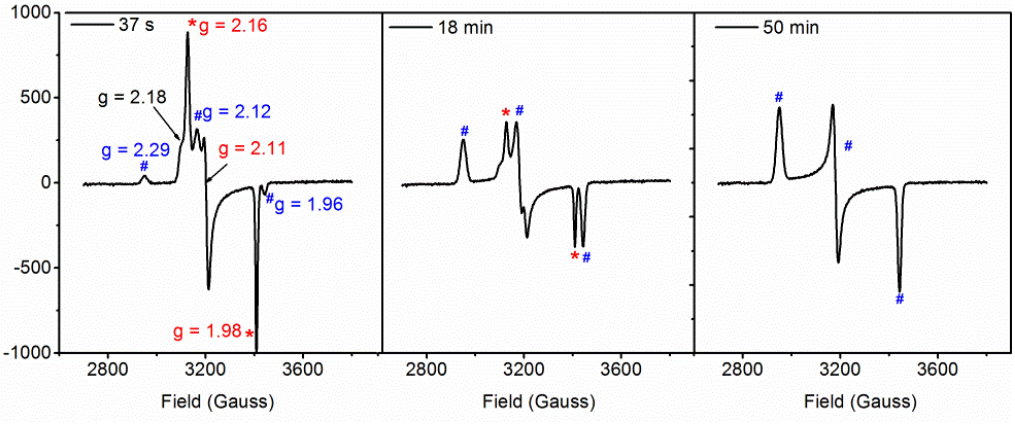

Figure 106. X-band EPR spectra (recorded at 77 K) of the reaction mixture of **2a** (1 mM) with 50 equiv H_2O_2 in methanol. (left) EPR spectrum 37 s after addition of H_2O_2, (middle) 18 min after addition, (right) after complete decay of Fe^{III}-OOH (50 min). Microwave Frequency 9.46 GHz, Power 63.5 mW.

Notably, both the maximum extent of formation of **3** and the time between addition of H_2O_2 and the start of the subsequent decrease in the absorbance of **3** are dependent on the initial concentration of H_2O_2 (**Figure 105**). These data indicate that H_2O_2 consumption is relatively similar to the rate of formation **3** from **5a**. The rate of decrease of the absorbance due to **3** is independent of the initial H_2O_2 concentration (**Figure 107**), because the decay occurs only after essentially all of the H_2O_2 has been consumed, confirmed by Raman spectroscopy (λ_{exc} = 785 nm, **Figure 108**). Time resolved Raman spectroscopy shows that the concentration of H_2O_2 decreases from t = 0 while the resonantly enhanced bands of **3** (Fe^{III}-OOH) at 632, 650, 670 and 798 cm^{-1} do not decrease in intensity until the signal (υ(O-O)) from H_2O_2 at 872 cm^{-1} has decreased to near-stoichiometric levels at least (i.e. below the limit of detection of ca. 10 mM, **Figure 109**).

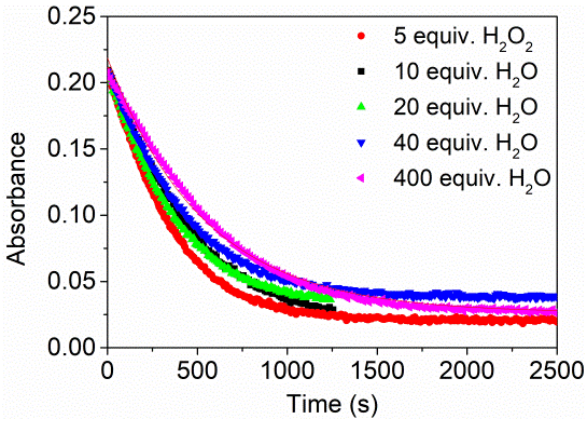

Figure 107. The decay of $[(N4Py)Fe(III)(OOH)]^{2+}$ after the threshold (absorbance at 550 nm decrease to 0.2,) of the reaction of **1** (0.56 mM) with H_2O_2 (2.5 to 50 mM)) at 21 °C.

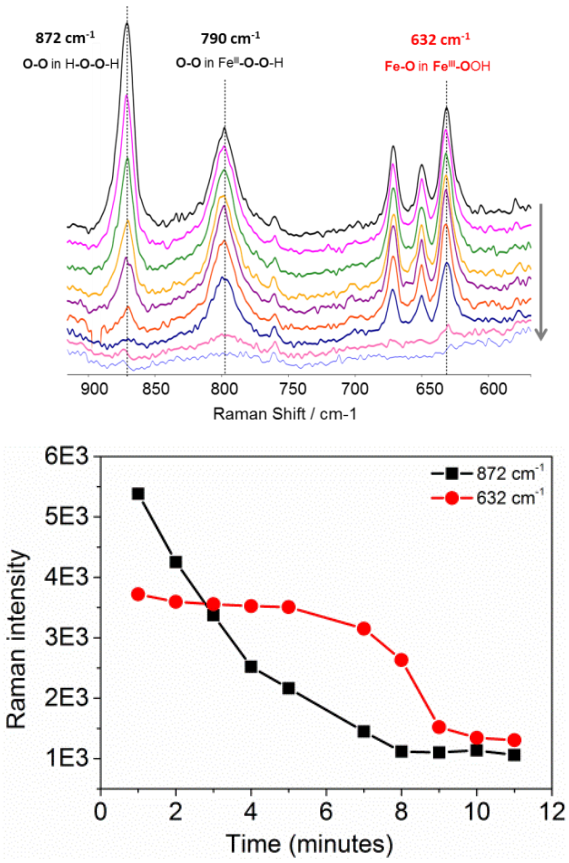

Figure 108. (left) Raman spectra of **1** (ca. 5 mM) in methanol over time after addition of 50 equiv H_2O_2 at λ_{exc} = 785 nm and (right) change in intensity of Raman bands at 872 cm^{-1}(of H_2O_2) and 632 cm^{-1} (of **3**) over time at 21 °C. Spectra correspond to data points shown.

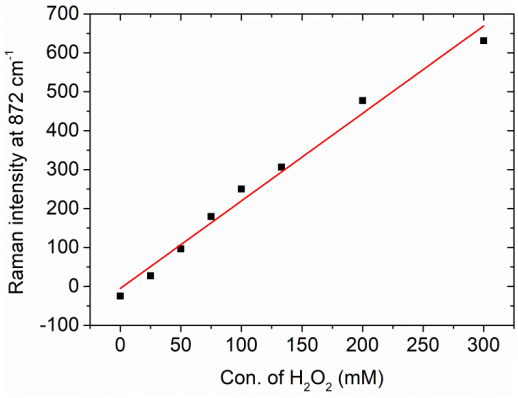

Figure 109. Calibration curve for Raman intensity at 872 cm^{-1} (λ_{exc} =785 nm) with respect to concentration of H_2O_2.

6.2.3 Regeneration of Fe^{III}-OOH and O_2 evolution

As for the absorption at 550 nm and its EPR signals, the characteristic Raman bands of **3** appear within the time resolution of the measurement (< 60 s) upon addition of excess H_2O_2, and maintain their intensity until the H_2O_2 has been consumed. These data are consistent with the continuous regeneration of **3** from $[(N4Py)Fe^{III}\text{-}OR)]^{2+}$ (where R = H or CH_3) and H_2O_2; i.e. that **3** is the resting state in the cycle and that the formation of **3** from **2** is a rapid equilibrium prior to the rate determining step in the reaction.

Headspace analysis by Raman spectroscopy (**Figure 110**) confirms generation of O_2 at a rate corresponding to the rate of decrease of H_2O_2.

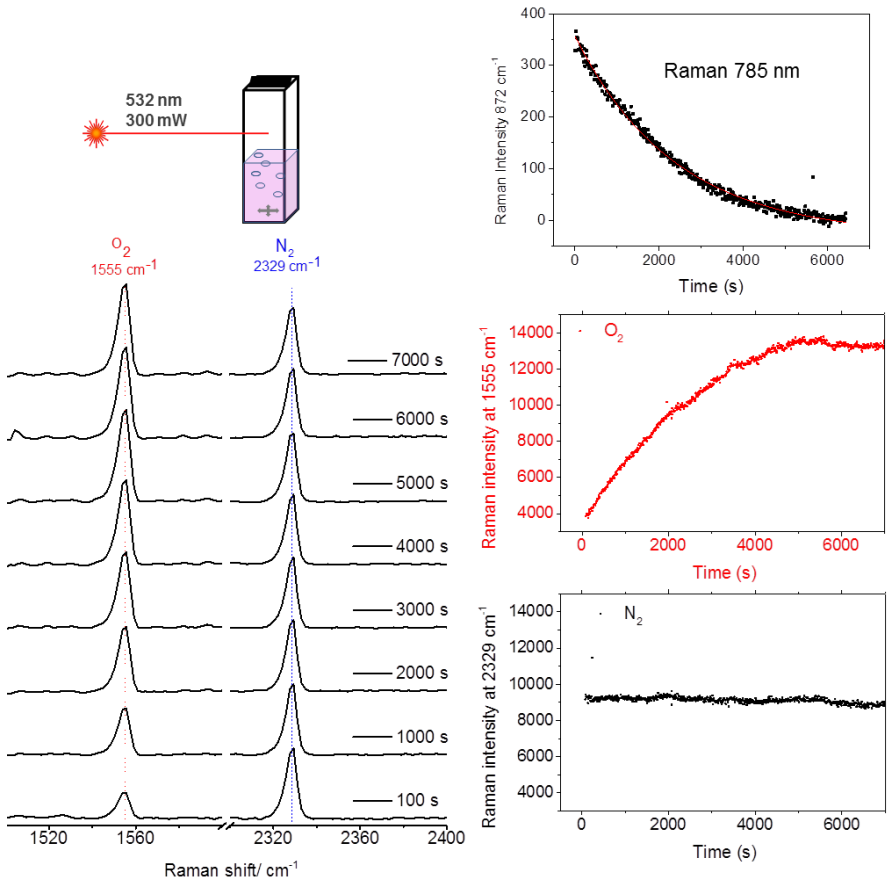

Figure 110. (Left) Raman spectra (λ_{exc} = 532 nm) obtained from the head space above the reaction mixture containing **1** (0.25 mM) and 200 mM H_2O_2 in methanol at 21 °C. (Right) Change in intensity of Raman band at 1555 cm^{-1} of O_2 (head space, red, λ_{exc} = 532 nm, internal reference was 2329 cm^{-1} band at N_2) and at 872 cm^{-1} for H_2O_2 (liquid phase, black, λ_{exc} = 785 nm).

The relation between the rate of consumption of H_2O_2 and concentration of **3** is apparent when H_2O_2 is present in excess (>50 equiv). The concentration of **3** remains constant (> 80% of total iron concentration) for a period of time, the duration of which is dependent on the initial concentration of **2** (**Figure 111**). The concentration of H_2O_2, determined by Raman spectroscopy, during this period shows an exponential decay (**Figure 112**). The observed rate constant (k_{obs}) for the decomposition of H_2O_2 is linearly dependent on the catalyst concentration (i.e. [**3**], **Figure 112**), with a second order rate constant of 0.8 M^{-1} s^{-1} at 21 °C (**Figure 112**). The rate constant is less than that for the formation of **3** (10.5 (± 0.1) M^{-1} s^{-1}) and thus in agreement with **3** as the resting state in the catalytic cycle under steady state conditions.

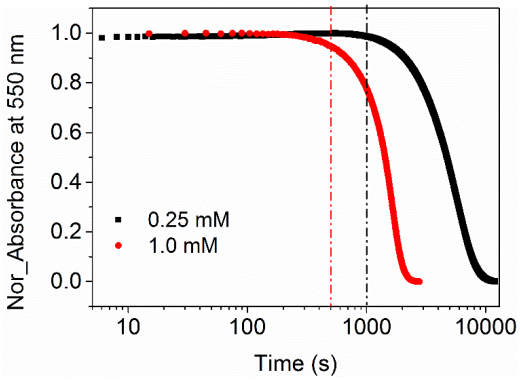

Figure 111. Normalized UV-vis absorbance at 550 nm of reaction of **1** (1.0 mM in red, 0.25 mM in black) with H_2O_2 (200 mM).

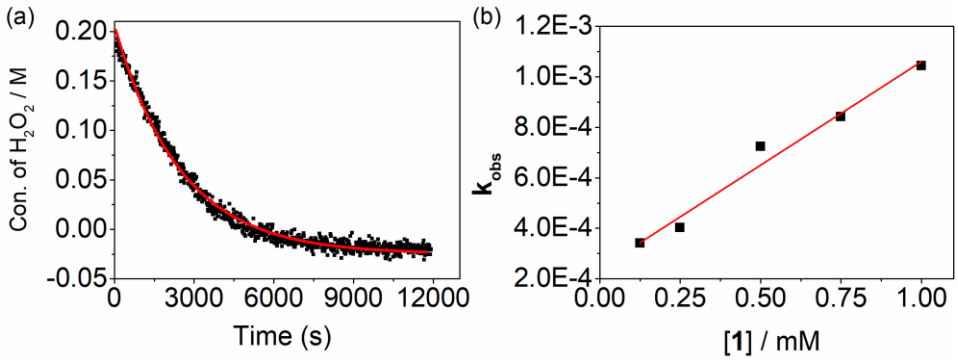

Figure 112. (left) Decrease in the concentration of H_2O_2 with time following addition of H_2O_2 (200 mM) to **1** (0.25 mM) at 21 ^{o} C. (right) Plot of the pseudo-first-order rate k_{obs} versus concentration of **1**.

6.2.4 Reaction of $[(N4Py)Fe^{IV}=O]^{2+}$ (4) with methanol and H_2O_2

The self-decay rate of **4** (prepared independently) due to reaction with solvent is low in acetonitrile,[27] but is significant in methanol (**Figure 113**). In methanol, the NIR absorbance of **4** decays exponentially over 1000 s with the concomitant production of 1 equiv of **5a** (Fe^{III}-OCH_3) and 0.5 equiv formaldehyde. The kinetic isotope effect for this decay in CD_3OD is ca. 10,[31](**Figure 113**). OH/OD exchange has no effect on this rate, which is consistent with the competence of **4** in the oxidation of methanol with a rate determining hydrogen atom abstraction (HAT) step at the C-H bond.

Addition of 1 equiv H_2O_2 to **4** (Fe^{IV}=O) in methanol results in conversion to **5a** (Fe^{III}-OCH_3) within 200 s, in agreement with data reported in acetonitrile (second order rate constant of 8 M^{-1} s^{-1} at 21 ^{o}C),[27] and ca. 10 times faster than the reaction of **4** with CH_3OH. However, in stark contrast with the 2:1 ratio of H_2O_2/**4** required in acetonitrile[27] for full reduction of **4** to the Fe^{III} state, in methanol only 1 equiv H_2O_2 is required (**Figure 113**).

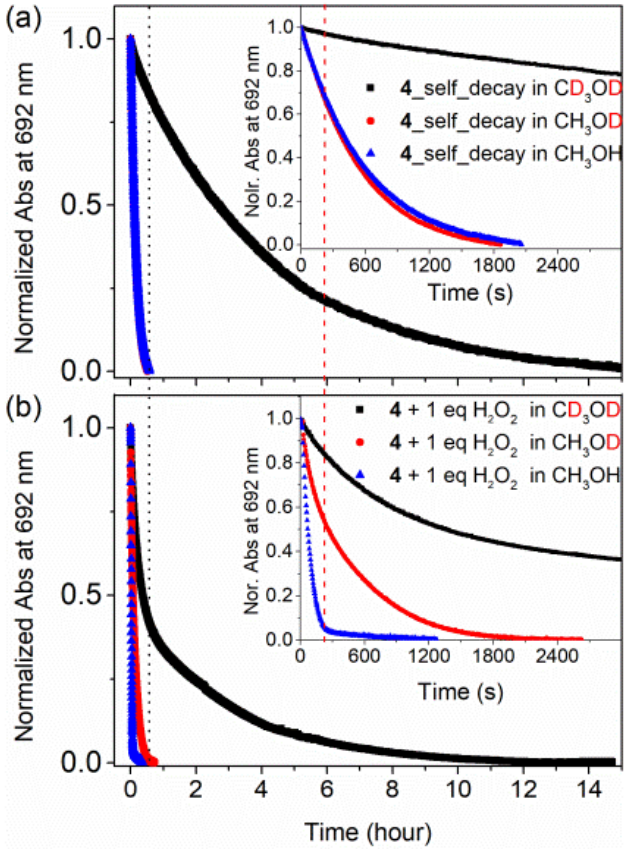

Figure 113. Absorbance of **4** (1 mM) at 692 nm in CH_3OH (blue), CH_3OD (red), and CD_3OD (black) with time in the (a) absence and (b) presence of 1 equiv H_2O_2.

The OH/OD kinetic isotope effect observed in the reduction of **4** with H_2O_2 is masked to some extent by the competing reaction of **4** with CH_3OD (vide supra), but is nevertheless consistent with a HAT mechanism.

In CD_3OD, deuterium atom abstraction (from C-D) by **4** does not occur to a significant extent on the time scale of the reaction of **4** with 1 equiv D_2O_2 and consequently the initial rate (< 0.5 h) represents better the latter reaction. Examination of the decay in absorbance at 692 nm provides an important observation. In contrast to that observed in CH_3OH and CH_3OD, in CD_3OD the decay of **4** is biphasic with an initial fast phase over 1000 s, during which all of the D_2O_2 is consumed followed by a slower phase in which the rate of decay of **4** is essentially the rate of its reaction with CD_3OD. These data indicate that D_2O_2 is reduced through an alternative pathway, i.e., the Fe^{III} species formed initially competes with **4** in the reduction of D_2O_2. The reduction in efficiency, in terms of number of equivalents of hydrogen peroxide needed to reduce **4** is similar to that observed in acetonitrile.[27]

With excess H_2O_2 (40 equiv) in CH_3OH, the characteristic NIR absorbance of **4** disappears over 10 s, while that of **3** (Fe^{III}-OOH, **Figure 114**) appears concomitantly. These data indicate that the reduction of **4** to **5a** by H_2O_2 is followed by ligand exchange with H_2O_2 to form **3**. Thereafter, the spectral changes are essentially the same as observed upon addition of H_2O_2 to **1** in methanol.

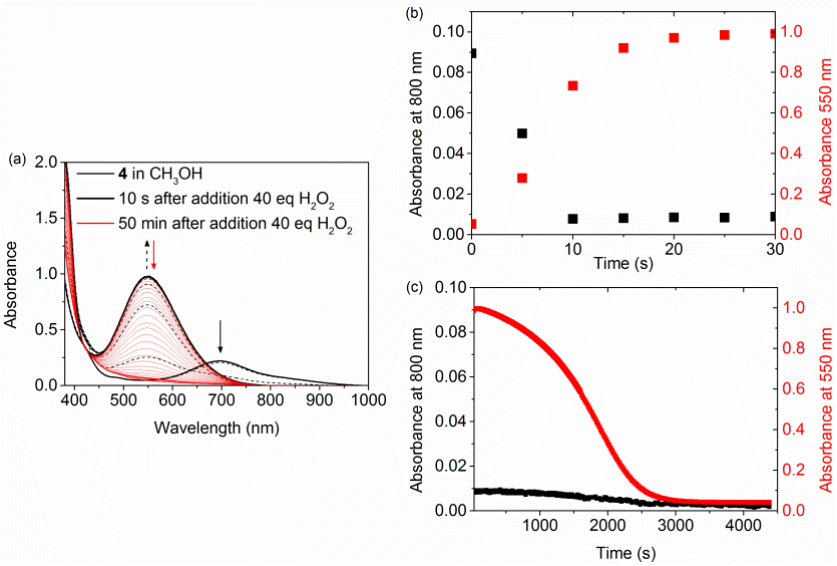

Figure 114. (a) UV-vis absorption spectrum of **4** (1 mM) after addition of 40 equiv H_2O_2 in CH_3OH. The changes of the absorbance at 550 nm (black) and 800 nm (red) between 0 - 150 s (b) and the changes after 150 s (c) are shown separately.

(3) $2[(N4Py)Fe^{IV}(O)]^{2+} + H_2O_2 \longrightarrow 2[(N4Py)Fe^{III}(OH)]^{2+} + O_2$

In summary, the rate of reaction of **4** follows the order H_2O_2 (in CH_3OH) > D_2O_2 (in CH_3OD) > D_2O_2 (in CD_3OD). Notably, the presence of even 1 equiv of H_2O_2 precludes the presence of **4** in methanol, rationalizing the fact that **4** can be observed only when the concentration of H_2O_2 is sub-stoichiometric. The rate of reduction of **4** by H_2O_2 in acetonitrile was reported by Braymer et al.[27] to be insensitive to deuteration (i.e. D_2O_2). In retrospect this observation can be understood by considering the need for excess H_2O_2 in that case and that **4** is not the sole species capable of reacting with H_2O_2.

6.2.5 Mechanistic considerations

The paradigm for oxidation catalysis with complexes such as **1** and H_2O_2 is rapid oxidation to the ferric state and formation of hydroperoxido complexes (*e.g.*, $[(N4Py)Fe^{III}\text{-}OOH)]^{2+}$, **3**). Homolytic cleavage of the O-O bond in **3** yields $[(N4Py)Fe^{IV}{=}O]^{2+}$ (**4**) and a hydroxyl radical, both of which are responsible for oxidation of organic substrates. In the present case, only **3**, and not **4**, is observed in the presence of H_2O_2, which is consistent with the homolytic cleavage of the O-O bond in **3** as rate determining.

The efficiency in the oxidation of organic substrates is diminished substantially in the presence of excess H_2O_2 due to disproportionation to H_2O and O_2. In the present study, independently prepared **4** is shown to be reduced to the ferric state in methanol rapidly upon addition of H_2O_2. Hence, the fact that **4** is not observed in the presence of excess H_2O_2 can be ascribed to this reaction pathway ((b) in **Scheme 12**). Indeed, $[(N4Py)Fe^{IV}{=}O]^{2+}$ (**4**) reacts with H_2O_2 (k = 8 M^{-1} s^{-1}) much more rapidly than the observed rate of decomposition of H_2O_2 (k = 0.8 M^{-1} s^{-1}). However, for pathway (b) (**Scheme 12**) to be kinetically possible the rate of the O-O bond homolysis of **3** must also be sufficiently rapid to account for the rate of decomposition of H_2O_2.

In the present study several observations cast doubt on the validity of pathway (b). In methanol, the formation of **4** from **3** is observed once (nearly) all H_2O_2 has been consumed, however, the rate of this reaction is much lower (< 3.0 x 10^{-3} s^{-1}) than expected (**Figure 103**). DFT

calculations (vide infra) indicate that the cleavage of the O-O bond is substantially uphill, and is accompanied by a low barrier to return to **3** (and hence has an intrinsically substantial thermal barrier). Consequently the rate of formation of $[(N4Py)Fe^{IV}=O]^{2+}$ (**4**) is insufficient to account for the decomposition of H_2O_2 when present in excess. This conclusion holds the further consequence that the formation of **4** and hence the oxidation of organic substrates by **4** is not competitive with oxidation of H_2O_2 by **3** (pathway (a), **Scheme 12**). The consequence of this is that the oxidation of organic substrates is only competitive under conditions of low H_2O_2 concentration.

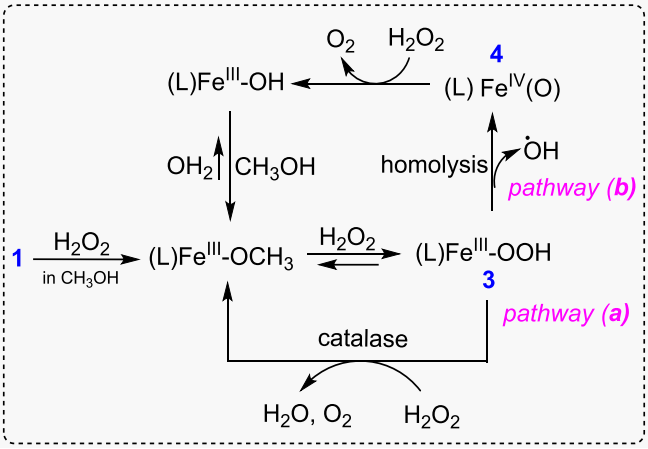

Scheme 12. Possible mechanism for the reaction of **1** with excess H_2O_2.

6.2.6 DFT calculations

The mechanism and comparison of two possible pathways for the reaction of **3** with H_2O_2 were explored through DFT calculations. Geometry optimization and frequency calculations were carried out at BP86-D_3/TDZP, with subsequent single point energies at S12g/TZ2P, including COSMO-ZORA self-consistently at all stages. All data are listed in Supporting information.

The doublet ground-state calculated for **3** is in accordance with experiments, however, for consistency, the reaction pathways a and b (**Scheme 12**) were calculated in all three possible spin states: doublet, quartet and sextet (**Figure 115**). For both pathways the reaction barriers are much lower in the low-spin state than the other two spin states, and hence the discussion below considered only the low spin states (**Figure 116** and **Figure 117**).

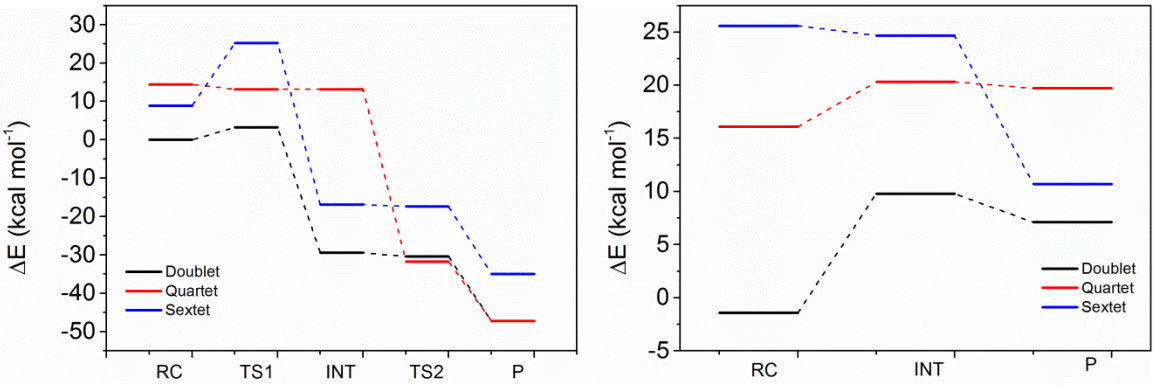

Figure 115. Comparison of energy profiles (in kcal mol^{-1}) of pathway a (left) and pathway b (right) in different spin states: doublet (black), quartet (red) and sextet (blue), as obtained at the S12g/TZ2P//BP86-D_3/TDZP level.

For the disproportionation pathway (a), the reactants, **3** + H_2O_2, form initially a reactant complex (RC) where the peroxide is bound to the iron complex weakly. This step is followed (in TS1) by hydrogen atom abstraction from the peroxide towards the distal OH group of **3**, and simultaneously cleavage of the O-OH bond of **3** takes place with a barrier of only 3.2 kcal mol^{-1}. In this TS, the O-OH bond in **3** elongates from 1.60 to 2.14 Å, together with a shortening of the H-(OH) distance to 1.45 Å. This is followed by a highly exergonic (-31.6 kcal mol^{-1}) completion of the hydrogen atom transfer process to form H_2O in the intermediate (INT). Simultaneously, the O-O bond of the peroxide shortens from 1.49 Å to 1.35 Å. Formation to the product from INT involves a second hydrogen atom abstraction (barrierless in terms of Gibbs free energy, -1.0 kcal mol^{-1}, +1.1 kcal·mol^{-1} in electronic energy) in which the remaining hydrogen of the peroxide is transferred to the oxygen coordinated to iron. This second HAT is exergonic by ca. -17.0 kcal·mol^{-1}, and finally leads to the products Fe^{III}-OH + H_2O + O_2.

In contrast, the homolysis pathway b, initially forms a similar weakly-bound complex in the RC_{homo}. However, the activation barrier (10.7 kcal mol^{-1}) for homolytic cleaving of the O-OH bond of **3** in TS_{homo} alone to form Fe(IV)=O is much higher than that in pathway a. The O-OH bond in **3** elongates from 1.51 to 2.63 Å with hardly any change in the structure of the peroxide, i.e., the peroxide does not participate actively in the reaction, but merely acts as hydrogen-bond donor. More importantly, the product for this homolytic pathway (b), P_{homo}, is so close in energy to the TS_{homo} (< 2 kcal mol^{-1}) that it readily undergoes the reverse reaction to the initial reactants.

These data are consistent with the observed low rate at which **4** forms from **3**, and the rapid consumption of H_2O_2 by direct reaction of **3** with hydrogen peroxide in the disproportionation pathway (a).

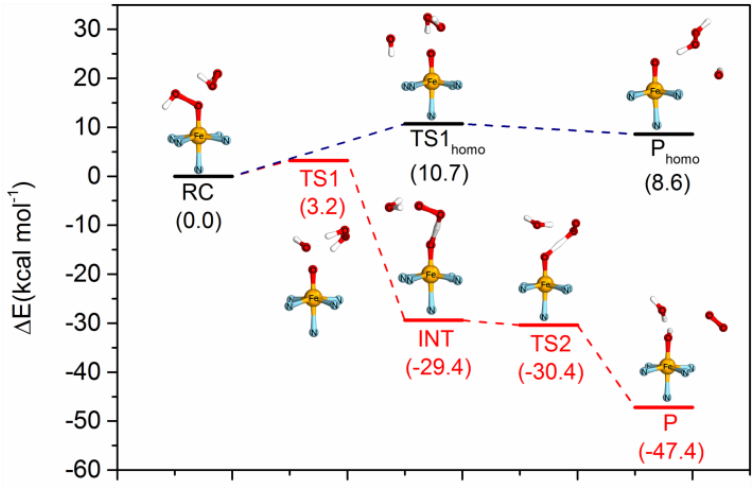

Figure 116. Comparison of energy profiles (in kcal mol^{-1}) of pathway (a) (catalase, in red) and pathway (b) (homolysis, in black), as obtained at the S12g/TZ2P//BP86-D_3/TDZP level.

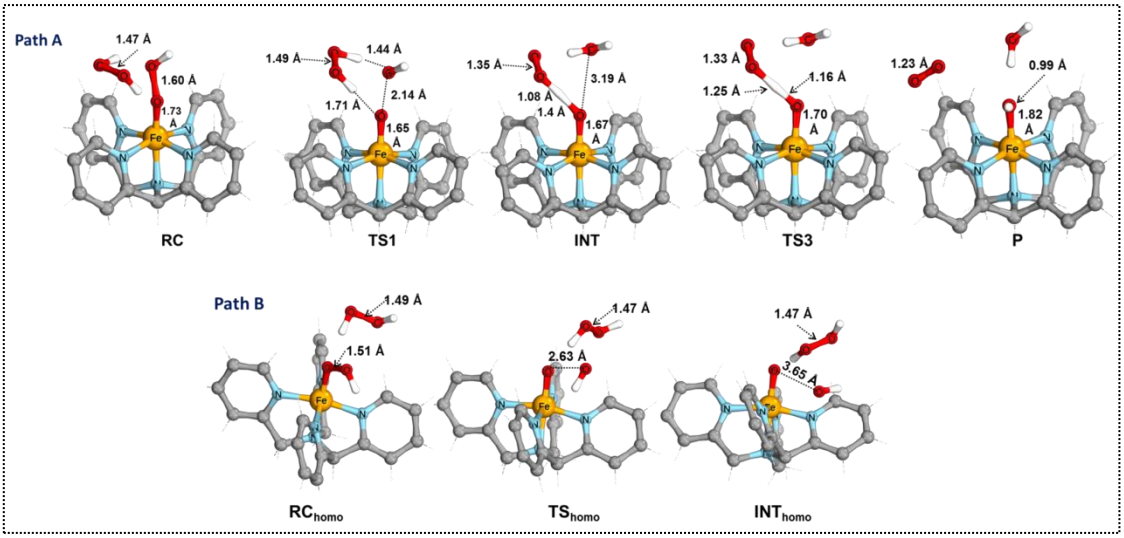

Figure 117. Geometries (bond distance in Å) for key species for both pathway (a) (catalase) and pathway (b) (homolysis).

In summary, there are two pathways that that should be considered for the decay of **3**. The first is a unimolecular homolysis to form **4** (Fe^{IV}=O) and a hydroxyl radical. This process is slow and only occurs at low concentrations of H_2O_2, in which H_2O_2 is outside of the solvation sphere of **3**. In this case, both **4** (Fe^{IV}=O) and $HO^{\bullet}$ are eventually formed and are responsible for the oxidation of organic substrates (i.e. methanol), and hence it is a productive reaction. In the presence of excess H_2O_2, i.e. within the solvation sphere of **3**, the formation of two H-bonds supports the breaking of the O-O bond of **3**, and either stabilizes (i) the formation of **4** ("insertion" of H_2O_2 into the O-O bond of **3** or (ii) through HAT from H_2O_2 to form water and $HOO^{\bullet-}$, and in a subsequent step, a second HAT from $HOO^{\bullet-}$ by Fe^{IV}=O leads to the formation of $[(L)Fe^{III}(OH)]^{2+}$ (**5b**) and dioxygen (see **Scheme 13**).

Our computational study shows that the barrier for reaction (i) is substantial and endergonic (10.7 kcal·mol^{-1}), even with stabilization through H-bonding with H_2O_2. The barrier for pathway (ii) is much lower (ca. 3.2 kcal·mol^{-1}), and leads to the generation of dioxygen (observed experimentally). Hence, in the presence of H_2O_2, **3** is almost exclusively transformed into **5b**, and with subsequent solvent exchange to **5a** (and subsequently through the exchange of methoxido by another H_2O_2 back to **3**). Therefore, in the presence of excess H_2O_2, disproportionation into H_2O and O_2 is the more energetically favored pathway.

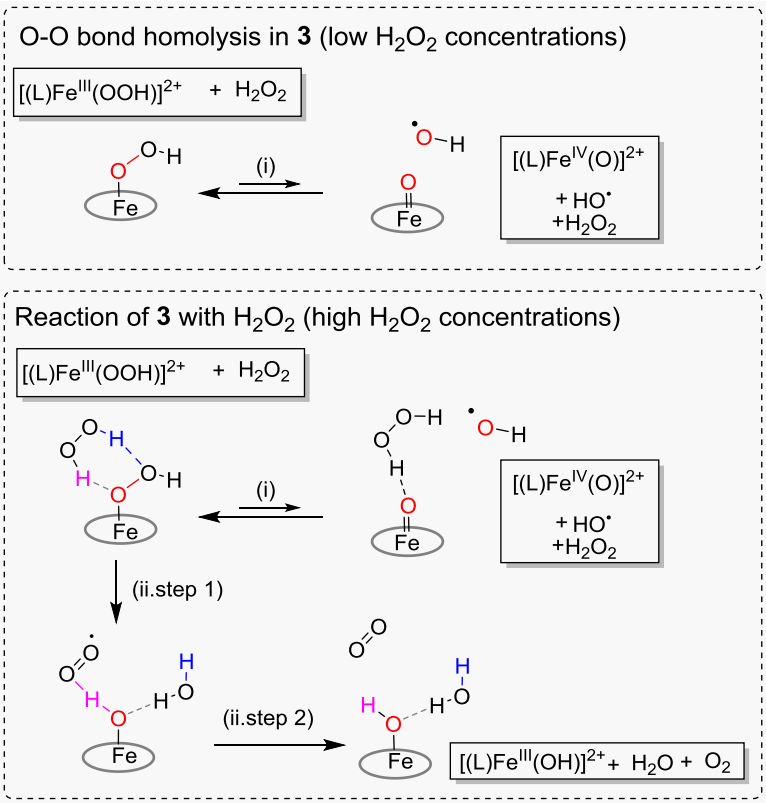

Scheme 13. Homolysis of the O-O bond in **3** to form **4** vs reaction of **3** with H_2O_2.

Regardless of the pathway, the observed reactivity presents a dichotomy towards the use of complexes such as **2a** for oxidation catalysis. **3** (Fe^{III}-OOH) does not appear to react directly with organic substrates, and hence formation of **4** (Fe^{IV}=O) and a hydroxyl radical from **3** through O-O bond homolysis is required. However, both **3** (Fe^{III}-OOH), and **4** (Fe^{IV}=O) react with H_2O_2 more readily than with organic substrates (e.g., methanol). Therefore, ideally the steady state concentration of H_2O_2 should be held as low as possible, yet still sufficiently high to generate **3** and, form **4** (Fe^{IV}=O)/$HO^{\bullet}$. Hence, the rate of addition of H_2O_2 should affect the relative efficiency of **2a** in the oxidation of organic substrates, as shown below for the oxidation of methanol.

6.2.7 Competition between the oxidation of methanol and H_2O_2 disproportionation catalyzed by 2a

The oxidation of methanol to methanal occurs concomitantly with the conversion of **4** (Fe^{IV}=O) to $[(N4Py)Fe^{II}\text{-}OCH_3)]^{2+}$ (vide supra). However, the rate of this reaction is sufficiently low to exclude it as being an important pathway for **2a** in the presence of excess H_2O_2 (i.e. both Fe^{III}-OOH and **4** (Fe^{IV}=O) react much more rapidly with H_2O_2 than with methanol). A number of competing kinetically competent pathways are thus available in the reaction of **2a** with H_2O_2 and variation in the steady state concentrations of reaction components should indicate the relative importance of each of these pathways.

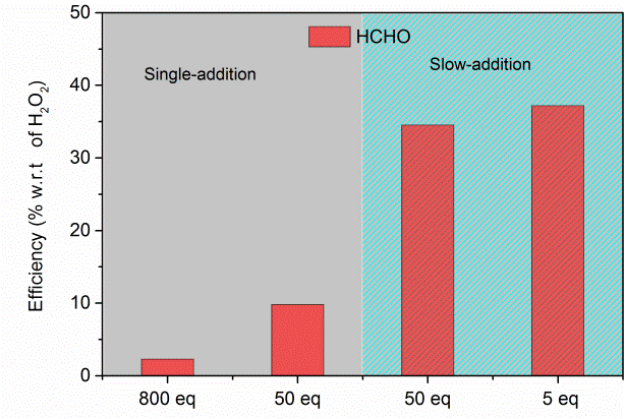

Figure 118. Oxidation of methanol (solvent) with H_2O_2 catalyzed by **1** (0.25 mM). HCHO was quantified colorimetrically. The number of equiv H_2O_2 is w.r.t to **2.** *Slow addition* of H_2O_2 indicates a rate of addition of 0.4 equiv. min^{-1}, bar 3/4.

With an 800 fold excess of H_2O_2, ca. 28 % of H_2O_2 is disproportionated to H_2O and O_2, with only 2 % generating formaldehyde (**Figure 118**, bar 1). Addition of fewer equivalents of H_2O_2 (bar 2) results in a substantial increase in the efficiency in the use of H_2O_2 to oxidize methanol, which increases further by addition of the same amount of H_2O_2 slowly. Adding fewer equivalents slowly over the same time does not increase efficiency further nor does a change in the concentration of the catalyst (0.25 vs 0.125 mM, bars 4 and 5, respectively), since overall conversion rates are controlled by the rate of addition. These data are consistent with the self-decay rate of **4** (Fe^{IV}=O), *vide supra*, setting the upper limit for the rate of addition of oxidant to achieve maximum efficiency.

6.3 Conclusions

The species accepted, i.e. Fe^{IV}=O, to be responsible for the oxidation of organic substrates by most non-heme iron catalysts is formed from an Fe^{III}-OOH precursor through O-O bond homolysis, liberating an hydroxyl radical concomitantly. Que and co-workers[2] have noted that in systems where low spin Fe^{III}-OOH species are generated (with excess H_2O_2) and observed, the corresponding Fe^{IV}=O species is not observed.

Here we show that in the case of non-heme N5 coordinated iron complexes that form observable Fe^{III}-OOH species, two key reasons can be invoked, to rationalize the absence of a corresponding Fe^{IV}=O species. The first is that even if it does form, it reacts rapidly and unproductively with H_2O_2 rather than with an organic substrate. Secondly, and unexpectedly, Fe^{III}-OOH (**3**) reacts more rapidly with H_2O_2 than it undergoes O-O bond homolysis to form an Fe^{IV}=O species in the first place.

Ligand exchange, i.e. Fe^{III}-OR to Fe^{III}-OOH (**3**), precedes the oxidation of both organic substrates (equation 2) and H_2O_2 (equation 4). In the present study we show that O-O bond homolysis is relatively slow and not competitive with the oxidation of H_2O_2 to O_2 by **3**. The reaction bifurcation seen for Fe^{III}-OOH presents a dichotomy in that H_2O_2 must be present in order to form Fe^{IV}=O (**4**), but the steady state concentration of H_2O_2 should be less than that of Fe^{III}-OOH (**3**), in order for O-O bond homolysis to form Fe^{IV}=O and an $HO^{\cdot}$ radical can take place and hence oxidation of organic substrates. Hence, efficiency w.r.t. oxidation of organic substrates

is increased, as observed in the present study, by maintaining low steady state concentrations of H_2O_2.

In conclusion, we show that in the oxidation of organic substrates by reactive iron species (Fe(IV)=O and Fe(III)OOH) competes with the reaction of these same species with H_2O_2 and hence wasteful disproportionation of the terminal oxidant. A substantial increase in oxidant efficiency is achieved by maintaining a pseudo steady state concentration of H_2O_2 that is below that of the catalyst itself. Furthermore, far from only being a meta-stable intermediate on route to an Fe^{IV}=O species, the Fe^{III}-OOH complex is kinetically competent in its reaction with H_2O_2. The conclusions reached in the present study have implications in regard to our approach to oxidation catalysis with iron catalysts with pentadentate ligands and in a wider perspective hold implications for the mechanisms invoked for catalase type reactions in both biomimetic and bioinorganic systems.

6.4 Experimental section

Synthesis. The ligand 1,1-di(pyridin-2-yl)-N,N-bis(pyridin-2-ylmethyl)methanamine (N4Py),[32] $[(N4Py)Fe^{II}(CH_3CN)O](ClO4)_2$ (**1**)[21,32,33] and $[(N4Py)Fe^{IV}=O](PF_6)_2$ (**4**)[31] were prepared as reported previously. Commercially available chemicals were purchased from Sigma Aldrich without further purification. All solvents used for spectroscopy were of UVASOL (Merck) grade.

Computational details

Computational studies were performed using ADF and QUILD,[34–36] as reported earlier.[37] Briefly, geometry optimization and frequency calculation were performed using an unrestricted density functional BP86-D_3[38–40] using a triple-zeta valence plus polarization basis set on iron combined with a double-zeta valence plus polarization on all other atoms (TDZP). Single-point energy calculations on these geometries were made with the S12g spin-state consistent functional[41,42] in a triple-zeta valence plus double polarization (TZ2P) basis set. Free energy corrections (ΔG) were obtained from the BP86-D_3 data and are corrected for zero point energy (ZPE), thermal and entropic corrections were made from frequency calculations at 298 K. The solvation energy was considered using methanol as a solvent with the COSMO solvation model as implemented in ADF.[43]

6.5 Acknowledgements

We thank Dr. Davide Angelone and Prof. Marcel Swart for the help with DFT calculations, Dr. Apparao Draksharapu Dr. Duenpen Unjaroen, Dr. Sandeep K. Padamati, and Dr. Ronald Hage for technical assistance and discussion, Prof. Carole Duboc for EPR studies and guidance in this projects. The Ministry of Education, Culture and Science of the Netherlands (Gravity program 024.001.035, WRB), Ubbo Emmius fund (AD), the European research council (W.R.B), COST association action CM1305 ECOSTBio, the labex arcane (ANR-11-LABX-003), MINECO (CTQ2014-59212-P and CTQ2015-70851-ERC, M.S.), GenCat (2014SGR1202, M.S.), FEDER (UNGI10-4E-801, M.S.), and the Chinese Scholarship Council (J.C.) are acknowledged for financial support.

6.6 References

(1) Costas, M.; Mehn, M. P.; Jensen, M. P.; Que, L. *Chem. Rev.* **2004**, *104* (2), 939–986.

(2) Ghosh, A.; Mitchell, D. A.; Chanda, A.; Ryabov, A. D.; Popescu, D. L.; Upham, E. C.; Collins, G. J.; Collins, T. J. *J. Am. Chem. Soc.* **2008**, *130* (45), 15116–15126.

(3) Roelfes, G.; Lubben, M.; Hage, R.; Que, Lawrence, J.; Feringa, B. L. *Chem. – A Eur. J.* **2000**, *6*

(12), 2152.
(4) Kim, Y. M.; Cho, K. Bin; Cho, J.; Wang, B.; Li, C.; Shaik, S.; Nam, W. *J. Am. Chem. Soc.* 2013, *135* (24), 8838–8841.
(5) Geng, C.; Ye, S.; Neese, F. *Angew. Chemie - Int. Ed.* 2010, *49* (33), 5717–5720.
(6) Park, J.; Lee, Y.-M.; Nam, W.; Fukuzumi, S. *J. Am. Chem. Soc.* 2013, *135* (13), 5052–5061.
(7) Rana, S.; Dey, A.; Maiti, D. *Chem. Commun.* 2015, *51* (77), 14469–14472.
(8) Draksharapu, A.; Angelone, D.; Quesne, M. G.; Padamati, S. K.; Gómez, L.; Hage, R.; Costas, M.; Browne, W. R.; de Visser, S. P. *Angew. Chemie Int. Ed.* 2015, *54* (14), 4357–4361.
(9) Park, J.; Morimoto, Y.; Lee, Y.-M.; Nam, W.; Fukuzumi, S. *Inorg. Chem.* 2014, *53* (7), 3618–3628.
(10) Rohde, J.-U. *Science* 2003, *299* (5609), 1037–1039.
(11) Rana, S.; Dey, A.; Maiti, D. *Chem. Commun.* 2015, *51* (77), 14469–14472.
(12) Nam, W.; Lee, Y.-M.; Fukuzumi, S. *Acc. Chem. Res.* 2014, *47* (4), 1146–1154.
(13) Cho, K.; Wu, X.; Lee, Y.; Kwon, Y. H.; Shaik, S.; Nam, W. *J. Am. Chem. Soc.* 2012, *134* (50), 20222–20225.
(14) Kumar, D.; Hirao, H.; Que, L.; Shaik, S. *J. Am. Chem. Soc.* 2005, *127* (22), 8026–8027.
(15) Kaizer, J.; Klinker, E. J.; Oh, N. Y.; Rohde, J. U.; Song, W. J.; Stubna, A.; Kim, J.; Münck, E.; Nam, W.; Que, L. *J. Am. Chem. Soc.* 2004, *126* (2), 472–473.
(16) Sheldon, R. A.; Arends, I. W. C. E.; ten Brink, G.-J.; Dijksman, A. *Acc. Chem. Res.* 2002, *35* (9), 774–781.
(17) Franke, A.; Van Eldik, R. *Chem. - A Eur. J.* 2015, *21* (43), 15201–15210.
(18) Solomon, E. I.; Wong, S. D.; Liu, L. V.; Decker, A.; Chow, M. S. *Curr. Opin. Chem. Biol.* 2009, *13* (1), 99–113.
(19) Lehnert, N.; Neese, F.; Ho, R. Y. N.; Que, L.; Solomon, E. I. *J. Am. Chem. Soc.* 2002, *124* (36), 10810–10822.
(20) Sam, J. W.; Tang, X.-J.; Peisach, J. *J. Am. Chem. Soc.* 1994, *116* (12), 5250–5256.
(21) Roelfes, G.; Lubben, M.; Chen, K.; Ho, R. Y. N.; Meetsma, A.; Genseberger, S.; Hermant, R. M.; Hage, R.; Mandai, S. K.; Young Jr., V. G.; Zang, Y.; Kooijman, H.; Spek, A. L.; Que Jr., L.; Feringa, B. L. *Inorg. Chem.* 1999, *38* (8), 1929–1936.
(22) Hirao, H.; Li, F.; Que Jr., L.; Morokuma, K. *Inorg. Chem.* 2011, *50* (14), 6637–6648.
(23) Li, F.; Van, H. K. M.; Meier, K. K.; Munck, E.; Que Jr., L. *J. Am. Chem. Soc.* 2013, *135* (28), 10198–10201.
(24) Li, F.; Meier, K. K.; Cranswick, M. A.; Chakrabarti, M.; Van Heuvelen, K. M.; Munck, E.; Que, L. *J. Am. Chem. Soc.* 2011, *133* (19), 7256–7259.
(25) Brown-Marshall, C. D.; Diebold, A. R.; Solomon, E. I. *Biochemistry* 2010, *49* (6), 1176–1182.
(26) Quiñonero, D.; Morokuma, K.; Musaev, D. G.; Mas-Ballesté, R.; Que, L. *J. Am. Chem. Soc*. 2005, 6548–6549.
(27) Braymer, J. J.; O'Neill, K. P.; Rohde, J. U.; Lim, M. H. *Angew. Chemie - Int. Ed.* 2012, *51* (22), 5376–5380.
(28) Draksharapu, A.; Li, Q.; Logtenberg, H.; van den Berg, T. A.; Meetsma, A.; Killeen, J. S.; Feringa, B. L.; Hage, R.; Roelfes, G.; Browne, W. R. *Inorg. Chem.* 2012, *51*, 900–913.
(29) Draksharapu, A.; Li, Q.; Roelfes, G.; Browne, W. R. *Dalton Trans.* 2012, *41* (42), 13180–13190.
(30) Decker, A.; Chow, M. S.; Kemsley, J. N.; Lehnert, N.; Solomon, E. I. *J. Am. Chem. Soc.* 2006, *128* (14), 4719–4733.

(31) Chen, J.; Draksharapu, A.; Harvey, E.; Rasheed, W.; Que, L.; Browne, W. R. *Chem. Commun.* 2017, *53* (91), 12357–12360.
(32) Lubben, M.; Meetsma, A.; Wilkinson, E. C.; Feringa, B.; Que, L. *Angew. Chemie Int. Ed.* 1995, *34* (13–14), 1512–1514.
(33) Draksharapu, A.; Li, Q.; Logtenberg, H.; van den Berg, T. A.; Meetsma, A.; Killeen, J. S.; Feringa, B. L.; Hage, R.; Roelfes, G.; Browne, W. R. *Inorg. Chem.* 2011, *51* (2), 900–913.
(34) Baerends, E. J.; Autschbach, J.; Berces, A.; Bo, C.; Boerrigter, P. M.; Cavallo, L.; Chong, D. P.; Deng, L.; Dickson, R. M.; Ellis, D. E.; Fan, L.; Fischer, T. H.; Fonseca Guerra, C.; van Gisbergen, S. J. A.; Groeneveld, J. A.; Gritsenko, O. V; Grüning, M.; Harris, F. E.; van den Hoek, P.; Jacobsen, H.; van Kessel, G.; Kootstra, F.; van Lenthe, E.; Osinga, V. P.; Patchkovskii, S.; Philipsen, P. H. T.; Post, D.; Pye, C. C.; Ravenek, W.; Ros, P.; Schipper, P. R. T.; Schreckenbach, G.; Snijders, J. G.; Solà, M.; Swart, M.; Swerhone, D.; te Velde, G.; Vernooijs, P.; Versluis, L.; Visser, O.; van Wezenbeek, E.; Wiesenekker, G.; Wolff, S. K.; Woo, T. K.; Ziegler, T. SCM: Amsterdam 20016.
(35) te Velde, G.; Bickelhaupt, F. M.; Baerends, E. J.; Fonseca Guerra, C.; van Gisbergen, S. J. A.; Snijders, J. G.; Ziegler, T. *J. Comput. Chem.* 2001, *22* (9), 931–967.
(36) Swart, M.; Bickelhaupt, F. M. *J. Comput. Chem.* 2008, *29* (5), 724–734.
(37) Padamati, S. K.; Angelone, D.; Draksharapu, A.; Primi, G.; Martin, D. J.; Tromp, M.; Swart, M.; Browne, W. R. *J. Am. Chem. Soc.* 2017, *139* (25), 8718–8724.
(38) Becke, A. D. *Phys. Rev. A* 1988, *38* (6), 3098–3100.
(39) Perdew, J. P. *Phys. Rev. B* 1986, *33* (12), 8822–8824.
(40) Grimme, S.; Antony, J.; Ehrlich, S.; Krieg, H. *J. Chem. Phys.* 2010, *132* (15), 154104.
(41) Swart, M. *Chem. Phys. Lett.* 2013, *580* (0), 166–171.
(42) Swart, M.; Gruden, M. *Acc. Chem. Res.* 2016, *49* (12), 2690–2697.
(43) Swart, M.; Rösler, E.; Bickelhaupt, F. M. *Eur. J. Inorg. Chem.* 2007, *2007* (23), 3646–3654.